jove

Line Shape Analysis of Dynamic NMR Spectra for Characterizing Coordination Sphere Rearrangements at a Chiral Rhenium Polyhydride Complex

Sarah M. Tadros[1], **Marina Mansour**[1], **Datta V. Naik**[1], **Gregory A. Moehring**[1]

[1] Department of Chemistry and Physics, Monmouth University

Corresponding Author

Gregory A. Moehring
gmoehrin@monmouth.edu

Citation

Tadros, S.M., Mansour, M., Naik, D.V., Moehring, G.A. Line Shape Analysis of Dynamic NMR Spectra for Characterizing Coordination Sphere Rearrangements at a Chiral Rhenium Polyhydride Complex. *J. Vis. Exp.* (185), e64160, doi:10.3791/64160 (2022).

Date Published

July 27, 2022

DOI

10.3791/64160

URL

jove.com/video/64160

Abstract

Dynamic solution nuclear magnetic resonance (NMR) spectroscopy is the typical method of characterizing the dynamic rearrangements of atoms within the coordination sphere for transition metal polyhydride complexes. Line shape fitting of the dynamic NMR spectra can lead to estimates for the activation parameters of the dynamic rearrangement processes. A combination of dynamic ^{31}P-{^{1}H} NMR spectroscopy of metal-bound phosphorus atoms with dynamic ^{1}H-{^{31}P} NMR spectroscopy of hydride ligands may identify hydride ligand rearrangements that occur in conjunction with a phosphorus atom rearrangement. For molecules that exhibit such a coupled pair of rearrangements, dynamic NMR spectroscopy can be used to test theoretical models for the ligand rearrangements. Dynamic ^{1}H-{^{31}P} NMR spectroscopy and line shape fitting can also identify the presence of an exchange process that moves a specific hydride ligand beyond the metal's inner coordination sphere through a proton exchange with a solvent molecule such as adventitious water. The preparation of a new compound, $ReH_5(PPh_3)_2$(*sec*-butyl amine), that exemplifies multiple dynamic rearrangement processes is presented along with line shape fitting of dynamic NMR spectra of the complex. Line shape fitting results can be analyzed by the Eyring equation to estimate the activation parameters for the identified dynamic processes.

Introduction

NMR spectroscopy is commonly used to characterize dynamic processes that occur within or between molecules. For many simple intramolecular rearrangements, estimation of $\Delta G^{\ddagger}$ is as straight-forward as measuring the frequency difference, Δv, between two resonances at the slow exchange limit and determining the coalescence temperature for those same resonances (**Figure 1**)[1]. The relationship,

$$\Delta G^{\ddagger} = 4.575 \times 10^{-3} \text{ kcal/mol} \times T_C [9.972 + \log (T_C/\Delta v)]$$

where T_C is the coalescence temperature for a pair of resonances that represent the slow exchange form of

a dynamic sample, can be used to solve for the free energy of activation for such a dynamic rearrangement. More complex dynamic systems require line shape fitting of dynamic NMR spectra or another NMR technique such as two-dimensional exchange spectroscopy (2D-EXSY) or two-dimensional rotating-frame Overhauser effect spectroscopy (2D-ROESY) to estimate activation parameters.

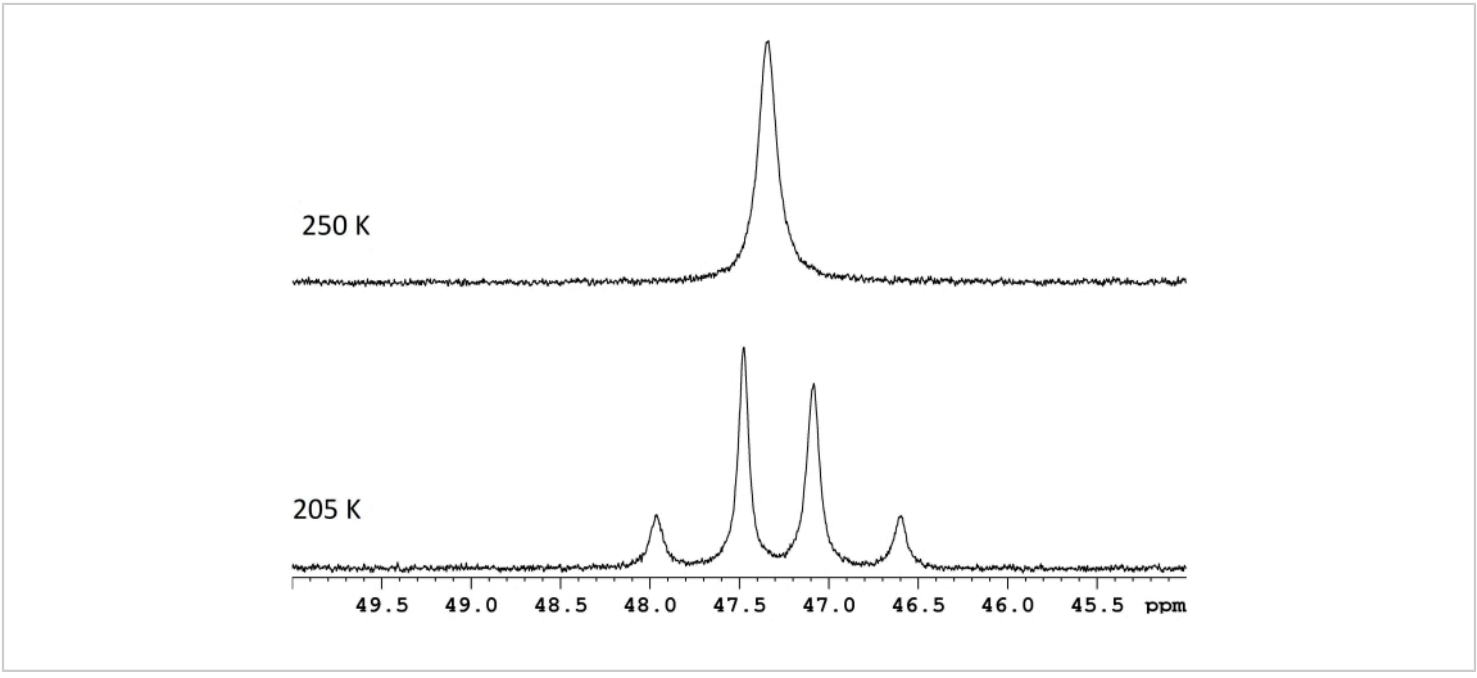

Figure 1: NMR spectra for a d_8-toluene solution of $ReH_5(PPh_3)_2$(*sec*-butyl amine) at two temperatures. The frequency difference between the two slow exchange doublets (lower trace, 117.8 Hz) and a coalescence temperature of 250 K (upper trace) correspond to an energy barrier ($\Delta G^{\ddagger}$) of 11.8 kcal/mol. Please click here to view a larger version of this figure.

Line shape fitting of dynamic NMR spectra is a common technique that has long been used for the estimation of activation parameters that describe dynamic rearrangements for substances with an activation energy of approximately 5 to 25 kcal/mol[2,3,4,5]. Determination of the energy barriers to proton exchange between water and amine molecules[6], the energy barrier to rotation about the C-N bond in dimethylformamide[7], or the general size of organic moieties[8] are only a few examples of the many properties that have been assessed through line shape fitting of dynamic NMR spectra. This manuscript demonstrates the use of line shape fitting to characterize the intermolecular and intramolecular dynamic processes that occur for the complex $ReH_5(PPh_3)_2$(*sec*-butyl amine). The goals of this and similar line shape fitting NMR experiments are to: 1) characterize all NMR observable intramolecular dynamic atom exchange processes if present, 2) identify and characterize NMR observable intramolecular dynamic atom exchange processes if present, 3) identify correlated intramolecular atom exchanges that occur for, in this example, both hydrogen and phosphorus atoms, and 4) for the example presented here, compare two published models for the dynamic processes that occur in the complex $ReH_5(PPh_3)_2$(*sec*-butyl amine).

Eight-coordinate rhenium(V) polyhydride systems are complex dynamic systems in which the ligands participate in multiple dynamic processes and the phosphorus atoms can participate in a single dynamic process that is a second aspect of a hydride ligand exchange process[9,10,11,12,13,14,15,16,17,18,19,20,21,22,23,24,25,26,27,28,29]. Eight-coordinate, pseudododecahedral, rhenium(V) polyhydride complexes adopt a molecular geometry (**Figure 2**), which can be described as a pair of orthogonal trapezoids of ligands[17,26]. The vertices on the long edges of the trapezoids are commonly labelled as B sites and, in rhenium polyhydride complexes, are usually the sites occupied by neutral two-electron donor ligands such as tertiary phosphines or amine ligands. The vertices on the short edges of the trapezoids are commonly labelled as A sites and are typically occupied by anionic, two-electron donor, hydride ligands. The room temperature NMR spectra of rhenium(V) polyhydride complexes are, typically, deceptively simple due to the several dynamic processes that occur in room temperature solutions.

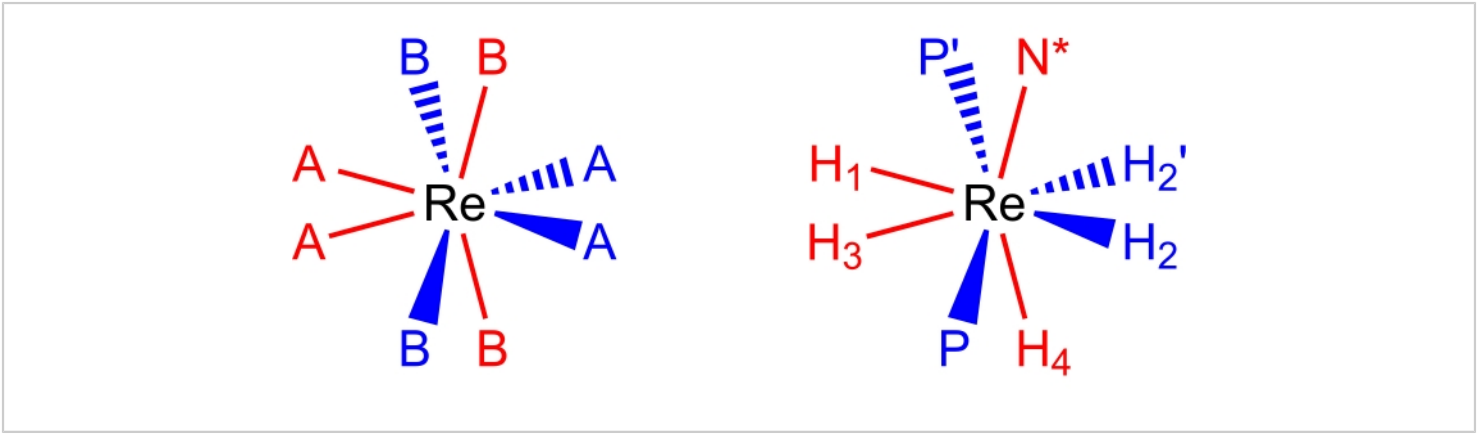

Figure 2: A dodecahedral coordination set (left) and the complex $ReH_5(PPh_3)_2$(*sec*-butyl amine) from the same perspective (right). The red-colored sites represent coordination sites that form a vertical trapezoid, and the blue-colored sites represent coordination sites that form a horizontal trapezoid. Please click here to view a larger version of this figure.

Complexes of the form $ReH_5(PPh_3)_2$(amine) are the most thoroughly studied class of rhenium polyhydride complexes with respect to dynamic processes[9,10,12,13,16,30,31]. Three dynamic processes (**Figure 3**) have been identified for $ReH_5(PPh_3)_2$(amine) complexes: 1) a proton exchange between the sole B site hydride ligand and a proton from a water molecule (adventitious or intentional)[9,13], 2) a turnstile exchange of a pair of A site hydride ligands with an adjacent B site hydride ligand[9,11,13,30,31], and 3) a steric inversion (or pseudorotation) that manifests itself as a pairwise exchange of the A site hydride ligands and a pairwise movement of the B site atoms to the opposite side of the rhenium center (as depicted in **Figure 4**)[4,5,6,8,26,27]. The movement of B site atoms to the opposite side of rhenium is observable by dynamic NMR spectroscopy as: 1) a process that makes the inequivalent 3 and 5 protons of N = pyridine equivalent at room temperature[10,30,31], 2) a process that causes the *E* and *Z* isomers of N = unsymmetrically substituted aromatic amine ligands to undergo fast exchange at room temperature[9,10,13,30,31], or 3) a process that

causes a fast exchange of the steric perspectives of a diastereotopic pair of phosphorus atoms with respect to a chiral center located on the amine ligand[9,30,31]. The previously unreported chiral complex $ReH_5(PPh_3)_2$(*sec*-butyl amine) provides an opportunity to generally describe the methods that can be used to identify and characterize the dynamic rearrangements of rhenium polyhydride complexes.

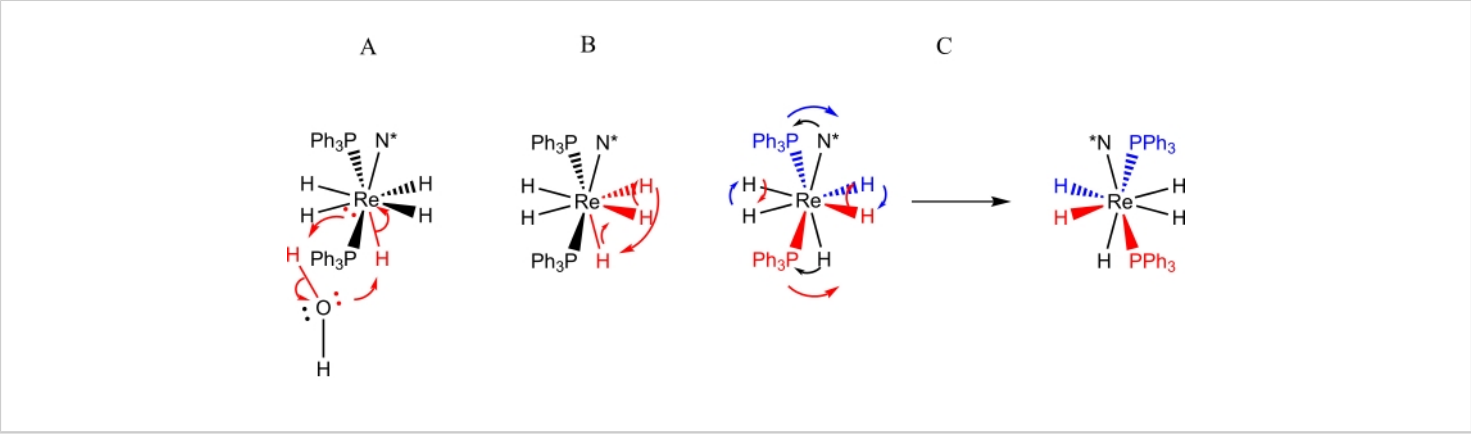

Figure 3: Representations of the dynamic processes that are observed by NMR spectroscopy for solutions of $ReH_5(PPh_3)_2$(*sec*-butyl amine). Representation A depicts the exchange of a single proton of adventitious water for the unique B-site hydride ligand. Representation B depicts the turnstile exchange of three adjacent hydride ligands, two of which reside in A site while the third is the unique B site hydride ligand. Representation C depicts both the pairwise exchange of A site hydride ligands as well as the steric inversion of the phosphorus atoms with respect to the chiral amine ligand (N*). It should be noted that the A site hydride ligand pairwise exchange does not require a shift of the A site hydride ligands to the opposite side of the rhenium center. Please click here to view a larger version of this figure.

For chemical systems such as rhenium polyhydride complexes, which exhibit a complex set of dynamic processes, line shape fitting of dynamic NMR spectra is the most used NMR technique to characterize the processes[9,11,13,16,21,29]. Two-dimensional EXSY[9,32] or 2D-ROESY[11] are alternative dynamic NMR techniques that can also be used to quantitatively characterize the dynamic processes. Two-dimensional EXSY spectra are typically measured in the slow exchange temperature domain; two-dimensional ROESY spectra are typically measured in the fast exchange temperature domain. Both two-dimensional techniques may require considerable time in the spectrometer for data acquisition, in that each of the techniques is acquiring a much larger data set, at a given temperature, than the one-dimensional data sets needed for line shape fitting analysis. Simple dynamic processes that are well understood, such as the dynamic exchange of the two methyl groups of dimethylformamide, can be readily characterized by any of the three NMR techniques. More complex systems, such as $ReH_5(PPh_3)_2$(*sec*-butyl amine), in which individual hydride ligands participate in multiple dynamic processes, or systems that are not necessarily well understood, such as a novel transition metal polyhydride complex which may or may not exchange protons between a hydride ligand and adventitious water, are more easily quantitatively characterized by the line shape fitting NMR method than by the two-dimensional

NMR methods. Unlike the two-dimensional NMR methods, the line shape fitting method provides an easily interpretable visualization of the match between a tested model and the experimental data as well as visual evidence of an exchange that moves a hydride ligand beyond the inner coordination sphere of rhenium. Based upon peak heights and peak shapes in slow exchange spectra, even a complex dynamic system such as $ReH_5(PPh_3)_2$(*sec*-butyl amine) can lead to an easily tested initial set of exchange models. Additionally, when multiple theoretical models have been reported for a molecular transformation, line shape fitting of dynamic NMR spectra can allow for a visual comparison of each model versus observed spectra.

Beyond the three NMR techniques mentioned above, isotopic substitution NMR experiments involving D_2O or HD have been used to qualitatively demonstrate intermolecular exchange of atoms for complex rhenium polyhydride systems, but have not been used for quantitative characterizations[9,33,34,35]. Theoretical calculations present an additional method for characterizing the dynamic processes of complex dynamic systems[30,31,36]. Theoretical calculations have the advantage over line shape fitting in that they can be used to differentiate between possibilities that cannot be distinguished by line shape fitting analysis. For example, theoretical calculations have been used to describe an exchange that involves three adjacent hydride ligands on certain rhenium(V) complexes as a turnstile exchange of all three hydride ligands, rather than an alternating pair of pairwise exchanges with each pairwise exchange including a unique hydride ligand and one of two chemically equivalent hydride ligands[30,31]. The results of theoretical calculations are typically compared to experimentally observed quantitative characterizations from one of the three NMR techniques mentioned above as a check on the validity of the calculated results.

Line shape fitting of dynamic NMR spectra takes advantage of the change in the appearance of NMR spectra that occurs when NMR-active nuclei move between different chemical environments during an NMR measurement. Slow exchange NMR spectra (spectra with independent Lorentzian resonances for each set of exchanging nuclei) occur at temperatures where the frequency difference between resonances for nuclei that exchange is large compared with the rate of exchange of the nuclei[37]. Fast exchange NMR spectra (spectra with a single Lorentzian resonance for exchanging nuclei) occur at temperatures where the rate of exchange of the nuclei is much greater than the frequency difference between the slow exchange resonances[37]. Intermediate exchange rates occur for temperatures between the slow exchange temperature domain and the fast exchange temperature domain[37]. If the fundamental parameters of Larmor frequency, chemical shift of the exchanging nuclei, coupling constants (if any) for the exchanging nuclei, and relative populations of each nucleus type are known, rate constants for putative exchanges between nuclei can be determined by comparing simulated spectra to observed spectra at several intermediate temperatures. Good fits for simulations at several temperatures result in temperature and rate constant data that can be used with the Eyring equation to estimate activation parameters for the putative exchange(s). Results from the method have been found to be both accurate and reproducible.

Protocol

1. Sample preparation

1. Preparation of $ReH_7(PPh_3)_2$[35]

    1. Combine 0.15 g of sodium borohydride and 0.41 g of $ReOCl_3(PPh_3)_2$ in a two- or three-necked 100 mL round-bottomed flask fitted with a rubber septum and gas port, or a 100 mL Kjeldahl flask (with a side arm gas port) fitted with a rubber septum (**Supplementary Figure 1**).

    2. Add a spin bar to the reaction vessel.

    3. In a fume hood, use a piece of rubber pressure tubing to connect the gas port of the reaction vessel with one of the stopcocks of a dual glass manifold for vacuum and nitrogen gas. Connect the glass vacuum manifold to a vacuum pump with rubber pressure tubing and connect the glass nitrogen manifold to a regulated nitrogen gas cylinder.

    4. Connect the exit gas from the nitrogen gas manifold to a stopcock that can be used to direct the vented gas through either a 2 cm column of mineral oil or a 2 cm column of mercury.

    5. Open the tap on the nitrogen cylinder and adjust the pressure on the flowing gas to 34 pounds per square inch. Vent the nitrogen gas flow through the mercury bubbler.

    6. Evacuate the gas inside the reaction vessel by adjusting the stopcock on the glass manifold to connect the vessel to the vacuum manifold. Fill the reaction vessel with nitrogen gas by changing the glass manifold stopcock so that it connects the gas manifold with the reaction vessel.

    7. Repeat steps 1.1.5 and 1.1.6 two more times to completely replace the air in the reaction vessel with nitrogen gas. Chill the flask and its contents in an ice bath.

    8. Add 8 mL of deoxygenated water and 8 mL of deoxygenated tetrahydrofuran to the solids in the reaction vessel *via* a syringe. Switch the gas-venting stopcock so that the gas vents through the mineral oil bubbler. Stir the suspension mildly in the ice bath for 15 min. Remove the reaction vessel from the ice bath after the initial 15 min of stirring.

    9. Allow the mixture to continue stirring for another 45 min. Note the color of the reaction mixture as an indicator of when the reaction has completed. A tan to orange reaction mixture color (**Supplementary Figure 1**) indicates that the reaction has reached its end point.

    10. Upon achieving an orange to tan color for the reaction mixture, filter the mixture through a 30 mL medium sintered glass funnel. Wash the recovered solid three times each with 15 mL portions of water, methanol, and ethyl ether. Dry the solid under vacuum to remove any adsorbed solvent.

        NOTE: The reaction generally produces between 0.20 g and 0.25 g of product.

2. Preparation of $ReH_5(PPh_3)_2$(*sec*-butyl amine)

    1. Weigh 0.070 g of $ReH_7(PPh_3)_2$ and transfer it into a 50 mL single-necked round-bottomed flask that contains a spin bar. Fit the flask to a condenser equipped with a gas port. Deoxygenate the reaction

vessel using the pump and fill method from steps 1.1.3-1.1.7.

2. Add a volume of 8 mL of deoxygenated tetrahydrofuran to the reaction vessel *via* a syringe by cracking the joint between the round-bottomed flask and the condenser. Add a volume of 0.2 mL of *sec*-butyl amine in a similar fashion. Switch the gas-venting stopcock so that the gas vents to the mineral oil bubbler.

3. Heat the reaction mixture to reflux at 65 °C with a heating mantle connected to a variable AC transformer set to 40 on a scale of 0 to 140 for 40 min. Cool the reaction mixture to a temperature that allows for convenient handling of the flask.

4. Pour the reaction mixture into 25 mL of methanol in a 125 mL Erlenmeyer flask. Stir the mixture vigorously for 5 min. Add 5 mL of water to induce the formation of a flocculent yellow precipitate.

5. Collect the yellow precipitate by vacuum filtration in a sintered glass funnel. Wash the solid with 15 mL of methanol. Dry the solid under vacuum. Following this process, typical product yield is 0.035 g.

2. Acquisition and analysis of NMR spectra

1. Measurement of dynamic NMR spectra

    1. Prepare an NMR sample with approximately 8 mg of the complex$ReH_5(PPh_3)_2$(*sec*-butyl amine) in about 0.8 mL of d_8-toluene. Insert the sample into the instrument.

    2. Click on the **File** tab and select **New** from the choices that appear to open a dialog box that is used to build an NMR experiment.

    3. Build a ^1H experiment by completing the following steps.

        1. Assign a folder name for the new experiment by completing the **Name** input box with a unique file name. Assign an experiment number such as 1 for the ^1H experiment in the **EXPNO** box.

        2. Assign a process number of 1 for the experiment in the **PROCNO** box. Assign the folder into a directory using the dropdown list for **DIR**. Identify the solvent that the instrument will lock on from the dropdown **Solvent** choices.

        3. Choose the directory that contains the parameters for the ^1H experiment from the dropdown list of directories in **Experiment Dirs**. Select the **Proton** experiment from the choices in the dropdown **Experiment** list, and (optional) add a title for the data in the **Title** fill in box.

        4. Enter an **Eda** command in the command line and adjust the parameters as needed to meet the descriptions of the experiment provided in the second paragraph of the Discussion section below.

    4. Click on the **Window tab**, select **New Window** from the list, and repeat Steps 2.1.3.1-2.1.3.8 to prepare a ^1H-{^{31}P} experiment using an **EXPNO** value of 2 to differentiate the experiment from the ^1H experiment built previously.

    5. Click on the **Window tab**, select **New Window** from the list, and repeat Steps 2.1.3.1-2.1.3.8 to prepare a ^{31}P-{^1H} experiment using an **EXPNO** value of 3 to differentiate the experiment from the ^1H and ^1H-{^{31}P} experiments built previously (see

Supplementary Table 1 for detailed parameter information).

6. Enter a **Lock** command in the command line and select the d_8-toluene choice from the list. Click **OK** to accept the solvent choice. Enter an **Atma** command in the command line, if necessary, because of a variable nucleus X-band probe, to minimize reflected energy at the Larmor frequencies for ^{1}H and ^{31}P on the instrument.
7. Enter a **Ro** command on the command line, type a value of 20 into the box, and click on the **Start rotation** button. Enter a **Shim** command on the command line. Choose an appropriate autoshim routine such as **Topshim** from the list of shim routines and click the **Start** button.
8. Enter an **Rga** command on the command line. Choose the **Automatic Receiver Adjust** selection and click **OK**. In turn, measure the three spectra of the sample at room temperature using 64 scans for each spectrum with a **Go** command on the command line.
9. Transform the data from an experiment into a spectrum with an **Efp** command entered in the command line.
10. Adjust the phasing of the spectrum using the following commands.
    1. Click on the **Phase** tab followed by a click on the **Adjust Phase** tab. Hover the cursor over the **0** button on the phasing toolbar and hold the left mouse button down so that the **0** button turns to green.
    2. With the left mouse button held down, roll the mouse forward or backward until the baseline is flat over the entire spectrum and all of the resonances are displayed as absorbances (peaks rise above the baseline).
    3. If the baseline cannot be made flat with only the 0 button, adjust the 1 button as described in steps 2.1.10.1 and 2.1.10.2 as well as the 0 button, until the baseline is flat for the entire spectral window.
    4. Save the phase adjustment with the data by clicking on the **Save and Return** button on the phasing toolbar.
11. Adjust the number of scans for each measurement, as needed, based upon the signal-to-noise ratio in the spectrum, keeping in mind that signal-to-noise typically decreases at lower temperatures due to de-coalescence of the signals into individual resonances (**Figure 4**).
12. Prepare the spectrometer for temperature control as per instructions from the vendor. Enter a flow rate of 200 L/h for the cooling gas and a target temperature of 290 K for the probe. Allow the spectrometer to stabilize at the target temperature for 2 min. Increase the cooling gas flow rate, if needed, to 210 or 220 L/h to stabilize the temperature.
13. Shim the sample at 290 K as in Step 2.1.7. Change the file name for each of the previously measured spectra by adding the temperature to the end of the file name (Steps 2.1.2 and 2.1.3.1) and acquire a set of three spectra at 290 K.
14. Increase the cooling gas flow rate by ≥ 30 L/h, as needed to stabilize at the next temperature, and

decrease the target temperature by 10 K. Allow the spectrometer to stabilize at the next temperature for 2 min and then shim the sample as in Step 2.1.7. Measure the set of three spectra.

15. Repeat Steps 2.1.13 and 2.1.14 as needed to acquire spectra down to the lowest temperature desired.

    NOTE: A temperature of 200 K is usually sufficient for a complete set of data that is suitable for determining the activation parameters for the dynamic processes of the sample.

16. Warm the sample back to room temperature in increments of 10 K. Stabilize the temperature for 2 min at each temperature before warming the sample again to prevent damage to the glass liner of the probe.

2. Line shape analysis of the measured spectra

    1. Within the NMR program click on the command bar at the top left of thewindow and select **Open** from the dropdown menu. Select **Open NMR data stored in standard format**. Click **OK** to open the file explorer window for the program.

    2. Navigate to the folder for the data to be analyzed by line shape fitting. Select the file number that corresponds to the spectrum to be analyzed and click the **Display** button. The spectrum (if previously processed) or the free induction decay (FID) curve is displayed in the NMR software.

    3. Process the FID if necessary, by entering an **Efp** command (exponential multiplication, Fourier transformation, and phase correction) in the command line. Adjust the phase of the spectrum (Step 2.1.10).

    4. Adjust the baseline of the spectrum; if it is not flat across the entire spectrum then level with the 0-intensity line, as follows.

        1. Click the **Process** tab and then click the **Baseline** tab. Hover the cursor over the **A** button. Depress the left mouse button and roll the mouse forward or backward to level the red adjustment line with the left (downfield) end of the spectrum.

        2. If the baseline is still not level with the red adjustment line, repeat the process with the remaining letter buttons until the red adjustment line fits the baseline of the spectrum. Use the **save and return** button to save the adjustment when the red adjusted baseline matches the actual baseline.

    5. Select the **Analyze** tab within the NMR software. Within the analyze options, select the **Line Shapes** choice followed by the **Fit Dynamic NMR Models** choice.

    6. The spectrum is now displayed in the line shape fitting module window. Use the toolbars above the spectrum to adjust how the spectrum is displayed. The window to the left of the spectrum handles the line shape fitting of the spectrum.

    7. Adjust the spectrum display with the **Smooth Zoom Tool** so that the portion of the spectrum to be fitted is displayed in the spectrum window. Use the **Shift Spectrum Left and Right** toolbar button to center a portion of the spectrum in the display window.

    8. Access the chemical shift window for line shape fitting by selecting the **Spectrum** tab in the line shape fitting window.

9. Click on the **Edit Range** button. Enter the upper and lower chemical shifts for line shape fitting and click the **OK** button to accept those limits.

10. Start a model for line shape fitting by clicking on the **Spin System** tab in the line shape fitting window. Click on the **Add** button to allow for the building of a model spin system.

11. Unselect **LB** (for line broadening) and enter the value for line broadening manually with the mouse and the **LB** button on the line shape fitting toolbar.

12. Add the first nucleus into the model by clicking on the **Nucleus** tab followed by clicking on the **Add** button. A set of default values will appear for Nucleus 1. Adjust the chemical shift for Nucleus 1 by entering a value for chemical shift in the **Nu(iso)** box or with the **chemical shift** tool on the line shape fitting toolbar. NOTE: If the selection box is left in the checked form, the chemical shift of this nucleus will be varied to achieve the best fit. Unchecked variables will not be varied in the line fitting process.

13. Use the **Pseudospin** box for Nucleus 1 to input the number of equivalent nuclei for Nucleus 1 with each spin 1/2 nucleus equivalent to 0.5 in counting. Enter the sum of the spins into the **Pseudospin** box in order to account for all equivalent nuclei.

14. Use the **In Molecule** box to accommodate models that require more than a single molecule to participate in a dynamic process. Assign resonances that arise from different molecules to separate molecules using designations such as 1, 2, etc. for different molecules. For resonances that arise from a single molecule, assign 1 for all **In Molecule** values.

15. Add the second and all subsequent nuclei to the model by clicking on the **Nucleus** tab followed by clicking on the **Add** button. Include spin-spin coupling between nuclei by either entering the coupling in the appropriate **JN** box (where N is the nucleus with which the nucleus that is added is coupled, N = 1, 2, …) or by adjusting the **Scalar coupling** button on the line shape fitting toolbar.

16. Begin the process of describing the atom exchanges by clicking on the **Reaction** tab. Click on the **check box** if the rate constant for the exchange is to be varied in line shape fitting. Enter the number of nuclei to be exchanged (number with respect to their identifying tabs such as Nucleus 1 and Nucleus 2) into the **Exchanges** box for the first exchange in the model.

17. Describe the exchanges to be tested in the boxes below the **Exchanges** box. Define the exchanges between **Nucleus** tabs in the boxes below. A two Nucleus exchange would be entered as Nucleus 1 to Nucleus 2 and Nucleus 2 to Nucleus 1. Ensure that exchanges are cyclic in that if a nucleus is moved from Nucleus 1, another nucleus has to be moved into Nucleus 1.

18. Use the **Exchange speed** button on the line shape fitting toolbar to change the initial value of k in order to iteratively adjust the value of k, even if the check box is selected for the rate constant.

19. Add more exchanges to the model by clicking on the **Reaction** tab followed by clicking on the **Add** button. Add exchanges to the model as needed. Use the tools on the line shape fitting toolbar to adjust the

starting variables, including spectrum intensity to a good match for the spectrum to be fit.

20. Begin iterative line shape fitting by clicking on the **Start the Spectrum Fit** button on the line shape fitting toolbar. Continue iterative fitting until no change is found in the best overlap between spectrum and model or until 1000 iterations are reached. If fitting stops at 1000 iterations, continue further iterations with the **Start the Spectrum Fit** button. The model spectrum is displayed with the actual spectrum for comparison.

21. Record the best fit values from the appropriate tabs. Save the best fit spectrum by clicking on the **Spectrum** tab in the line shape fitting window followed by clicking on the **Save** button.

    NOTE: The best fit spectrum will be saved in the same folder as was used to collect the data. The best fit spectrum will be distinguished from the original data by being saved with a different processing number that is input when the save occurs.

22. Save the model used for the line shape fitting by clicking on the **Main** tab followed by clicking on the Save button. Enter a name for the model.

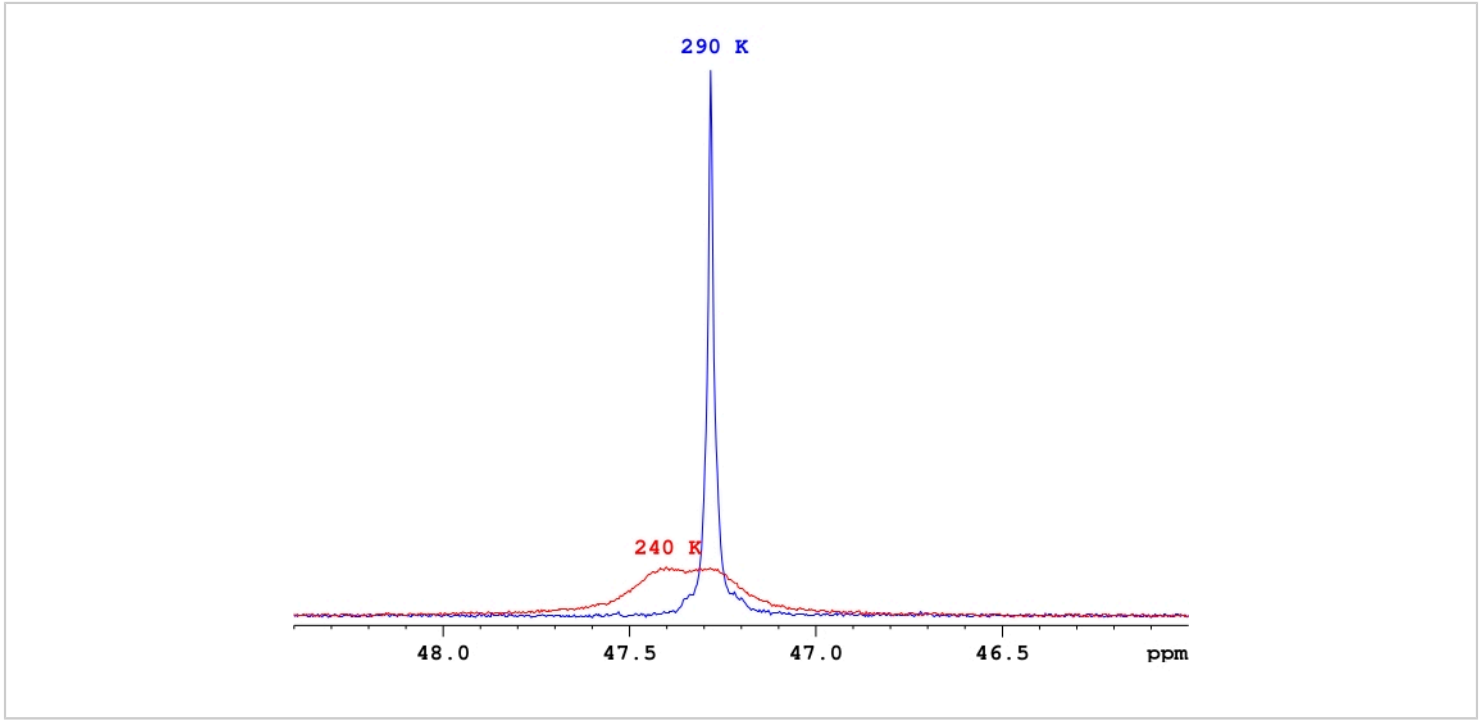

Figure 4: A comparison of ^{31}P-{^{1}H} signal intensities for a single sample of $ReH_5(PPh_3)_2$(*sec*-butyl amine) in d_8-toluene. A representative demonstration of the difference in signal intensities between a fast exchange single phosphorus resonance and a pair of phosphorus resonances near the coalescence temperature for those resonances. Please click here to view a larger version of this figure.

3. Determination of activation parameters from an Eyring plot [1]

1. Enter data from line shape fitting for one modelled dynamic process into a spreadsheet with the independent variable entered as 1/T and the dependent variable entered as ln(k/T).
2. Insert a scatter plot of the data into the spreadsheet. Add a trend line through the data. Use the slope and intercept of the trend line to solve for $\Delta H^{\ddagger}$ and $\Delta S^{\ddagger}$. The slope of the trend line is $-\Delta H^{\ddagger}/R$ while the intercept of the trend line is $\Delta S^{\ddagger}/R + 23.76$.
3. Solve for $\Delta G^{\ddagger}$ at a given temperature using the relationship

   $\Delta G^{\ddagger}_{(T)} = \Delta H^{\ddagger} - T\Delta S^{\ddagger}$.

   NOTE: For a simple exchange of two nuclei with resonances that coalesce, a check of the values of $\Delta H^{\ddagger}$ and $\Delta S^{\ddagger}$ can be performed by comparing $\Delta G^{\ddagger}$ calculated at the coalescence temperature with the value of $\Delta G^{\ddagger}$ that arises from the slow exchange frequency difference between resonances and the coalescence temperature.

Representative Results

The characterizations of both rhenium polyhydride products described in this manuscript are best accomplished by ^{1}H-{^{31}P} and ^{31}P-{^{1}H} NMR spectroscopy. In a room temperature d_6-benzene solution, the hydride ligand resonance of $ReH_7(PPh_3)_2$ appears as a binomial triplet at δ = -4.2 ppm with $^{2}J_{PH}$ = 18 Hz by ^{1}H NMR spectroscopy (**Supplementary Figure 2**). The same d_6-benzene solution will exhibit a singlet resonance at δ = 31.4 ppm by ^{31}P-{^{1}H} NMR (**Supplementary Figure 3**). In a d_8-toluene solution, the hydride ligand ^{1}H-{^{31}P} NMR resonance of $ReH_5(PPh_3)_2$(*sec*-butyl amine) appears as a broad singlet at δ = -4.83 ppm (**Supplementary Figure 4**). The same d_8-toluene solution will exhibit a singlet resonance at δ = 47.3 by ^{31}P-{^{1}H} NMR spectroscopy (**Supplementary Figure 5**). Common impurities that can occur for either sample are $ReH_5(PPh_3)_3$ ($\delta_{hydride}$ = -4.73; $^{2}J_{PH}$ = 18.8 Hz, quartet; $\delta_{phosphorus}$ = 34.16 measured in d_8-toluene) and $Re_2H_8(PPh3)_4$ ($\delta_{hydride}$ = -4.93; $^{2}J_{PH}$ = 9.3 Hz, pentet; $\delta_{phosphorus}$ = 42.79 measured in d_6-benzene).

Line shape fitting is generally straight-forward for dynamic ^{31}P-{^{1}H} NMR spectra of rhenium polyhydride complexes that do not exhibit *E* and *Z* isomers[10]. The best fit simulations and ^{31}P-{^{1}H} NMR spectra for the complex $ReH_5(PPh_3)_2$(*sec*-butyl amine) for several temperatures are shown in **Figure 5**. Only one model is needed to exchange phosphorus atoms on such complexes. When the phosphorus nuclei exhibit spin-spin coupling, as is the case with the complex $ReH_5(PPh_3)_2$(*sec*-butyl amine), that coupling must be included in the model for good results. To simulate ^{31}P-{^{1}H} NMR spectra measured at the coalescence temperature and above, the temperature dependence of the chemical shift difference between the two resonances must be tracked and used to estimate the chemical shifts of the nuclei at the coalescence temperature and above (**Figure 6**). Additionally, NMR spectra measured at temperatures near the freezing point of the solvent may exhibit broadening of resonances due to increased solvent viscosity and precipitation of the analyte. Spectra that exhibit such resonance broadening should not be included in determination of the rate constants that are subsequently used in Eyring plot determinations.

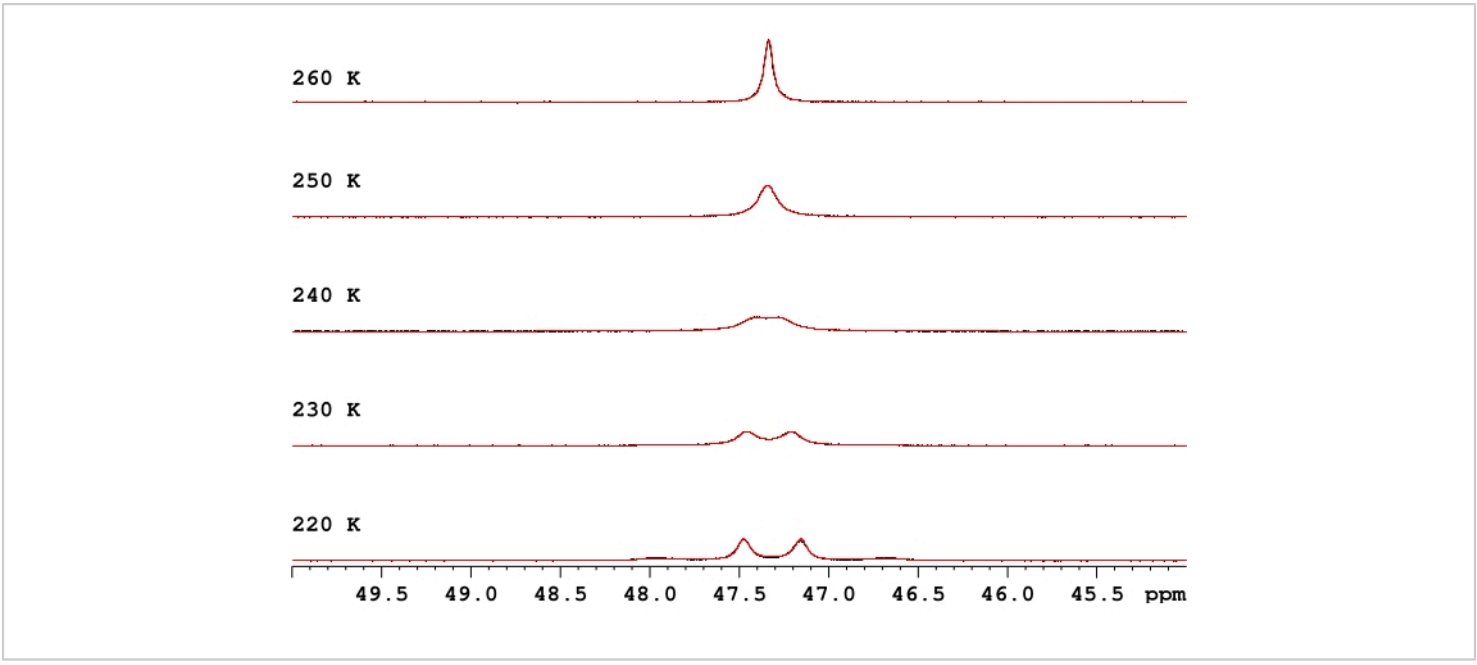

Figure 5. The $^{31}P\{^{1}H\}$ NMR spectra (black traces) and best fit simulations (red traces) for a d_8-toluene solution of $ReH_5(PPh_3)_2$(*sec*-butyl amine). The black traces show the coalescence of the two resonances that arise from the diastereotopic phosphorus atoms into a single resonance at higher temperatures. The red traces show a good match of the simulated spectra that arise from line shape fitting and the observed data. Please click here to view a larger version of this figure.

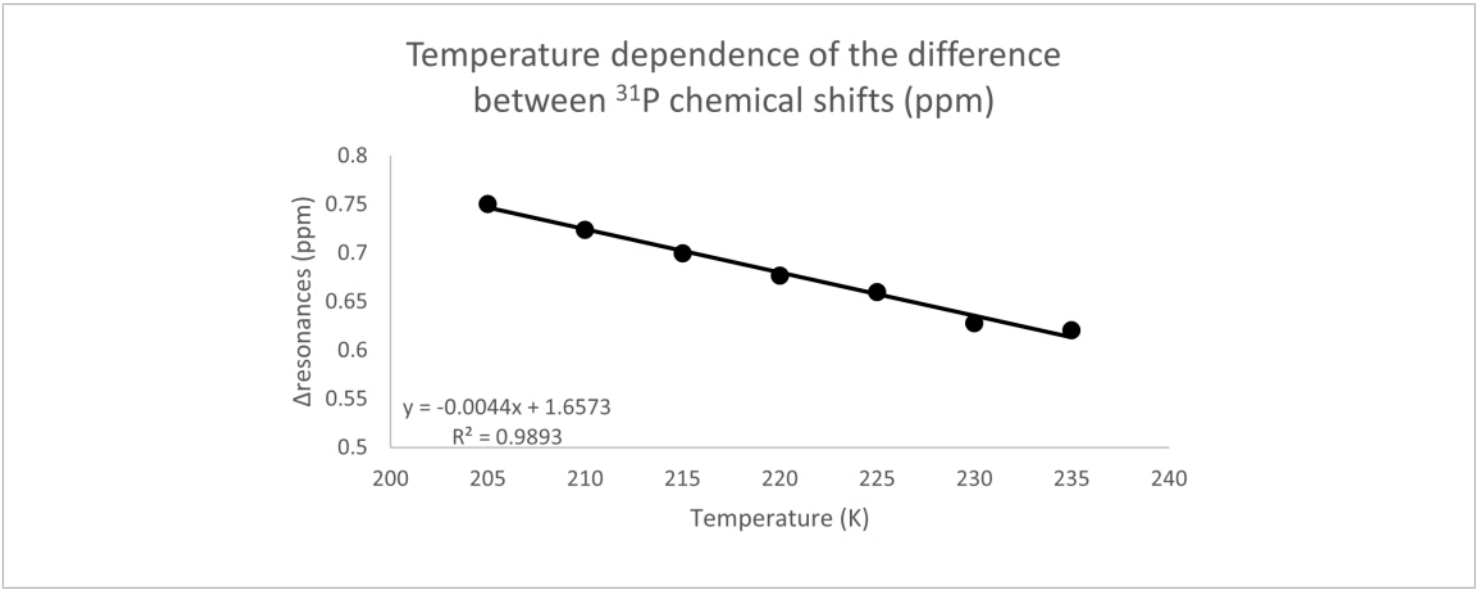

Figure 6. A plot of the temperature dependence of the difference in chemical shifts between the two ^{31}P-{^{1}H} resonances. An extrapolation of this line allows for estimation of the chemical shifts of the individual resonances at higher temperatures. Please click here to view a larger version of this figure.

Line shape fitting of the hydride region of dynamic ^{1}H-{^{31}P} NMR spectra is more challenging than line shape fitting for phosphorus resonances. Line shape fitting of hydride resonances requires more nuclei and more exchange models. Common hydride ligand exchange models that have been used for rhenium(V) polyhydride complexes include: 1) exchange between a pair of adjacent hydride ligands[16], 2) a turnstile exchange of three adjacent hydride ligands[9,11,13,30,31], 3) exchange between a specific hydride ligand and a proton from water[9,13], and 4) pairwise exchange of the A site hydride ligands on one side of rhenium with the A site hydride ligands on the other side of rhenium[9,13,31]. The latter exchange has been reported as a second aspect of the associated interconversion of *E* and *Z* phosphorus resonances or with the steric inversion of diastereotopic phosphorus resonances[13]. As such, the activation parameters and the rate constants for the latter hydride ligand exchange (if it occurs) should reflect the same values for the associated dynamic phosphorus process.

Line shape fitting can be used to test theoretical models of hydride ligand exchanges[13]. As with the phosphorus resonances mentioned above, the temperature dependence of the hydride resonances that will be modelled has to be determined so that chemical shifts can be adjusted for temperature drift. **Figure 7** shows the temperature dependence that was observed for the hydride resonances of an $ReH_5(PPh_3)_2$(*sec*-butyl amine) sample in d_8-toluene as well as the best linear fit equations for that drift. The models for line shape fitting of ^{1}H-{^{31}P} NMR spectra used chemical shifts that were calculated for each resonance even when the resonance frequency could be determined directly from the spectrum. Chemical shifts of the hydride resonances were not treated as variable when line shape fitting the hydride region of dynamic ^{1}H-{^{31}P} NMR spectra. **Figure 8** compares the

results of line shape fitting, based on a pairwise exchange of A site hydride ligands, a turnstile exchange of three adjacent hydride ligands, and a proton exchange between one proton of water and hydride ligand H4, with the observed hydride region of a series of ^{1}H-{^{31}P} NMR spectra collected from 225 K to 240 K.

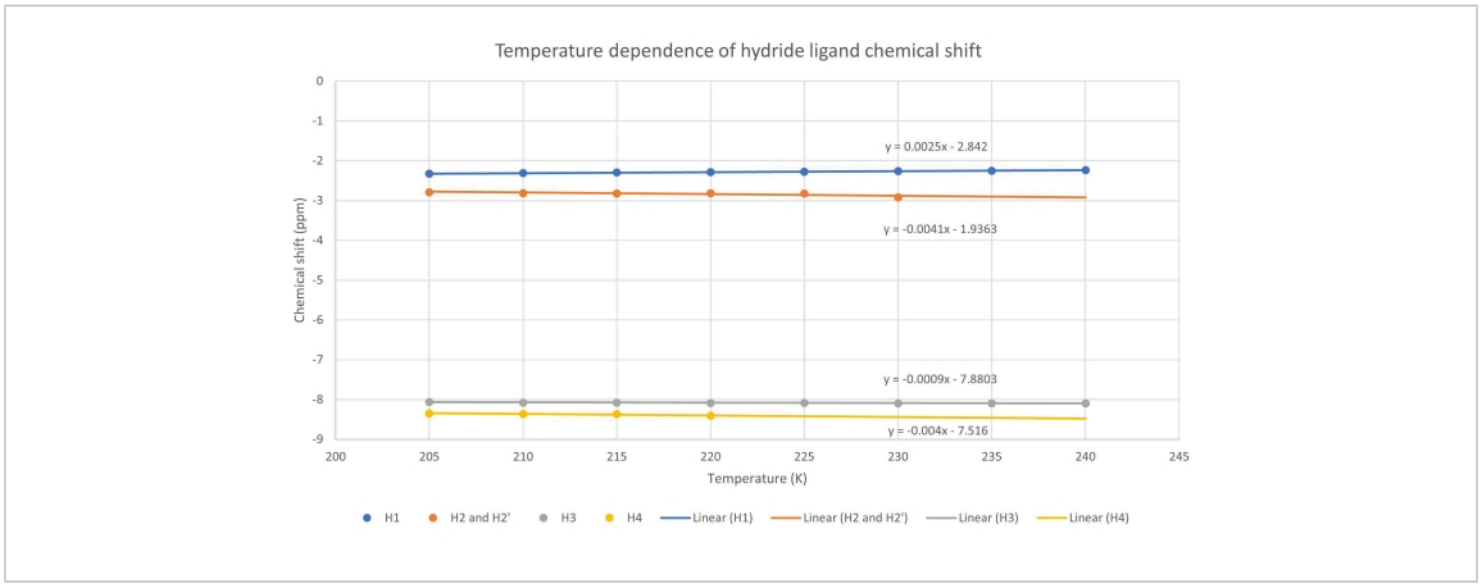

Figure 7. Best fit lines for the temperature dependence of each ^{1}H-{^{31}P} NMR hydride resonance. The chemical shifts calculated from the best linear fits were used in the models for line shape fitting of the observed spectra. Please click here to view a larger version of this figure.

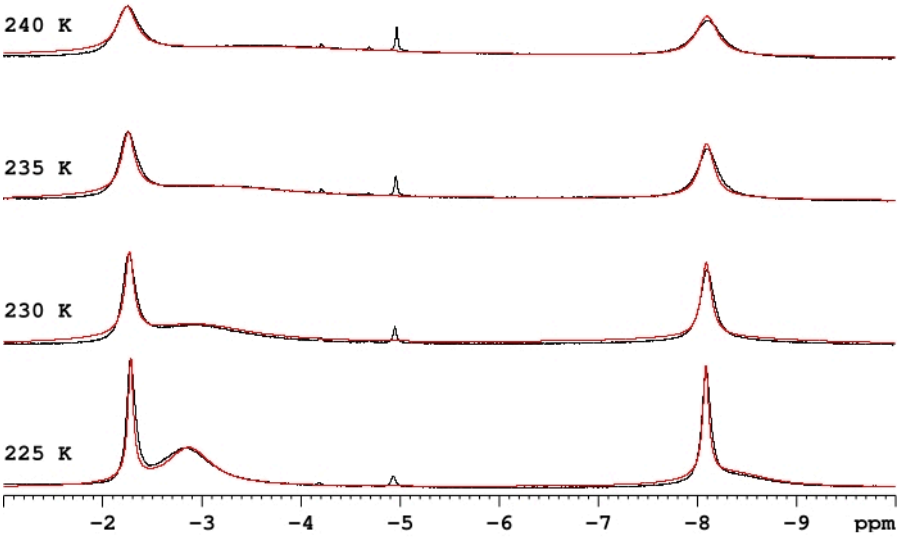

Figure 8. The hydride region of ^{1}H-{^{31}P} NMR spectra (black traces) and best fit simulations (red traces) for a solution of $ReH_5(PPh_3)_2$(*sec*-butyl amine). The spectra were measured on a d_8-toluene solution. Please click here to view a larger version of this figure.

Figure 9 displays best fits for two models of hydride ligand exchange for $ReH_5(PPh_3)_2$(amine) complexes in the hydride region of the 225 K ^{1}H-{^{31}P} NMR spectrum for a sample of $ReH_5(PPh_3)_2$(*sec*-butyl amine) in d_8-toluene. The line shape fits are based upon theoretical models of hydride ligand exchange for the compound $ReH_5(PPh_3)_2$(pyridine)[30,31]. Two aspects of the best fit spectra are important. First, the blue traces represent the best fits of the spectrum line shape based entirely on the reported exchange models. The blue traces indicate that a proton exchange between a specific hydride ligand and a proton from beyond the inner coordination sphere is missing. For this example, $ReH_5(PPh_3)_2$(*sec*-butyl amine) complex, the missing exchange includes a proton from adventitious water along with the unique B site hydride ligand. Second, the red traces indicate that when a proton exchange with water is included with either theoretical model, a good line shape may or may not be obtained. For the complex $ReH_5(PPh_3)_2$(*sec*-butyl amine), Model A generates the better fit for the observed spectrum. A comparison of rate constants for the steric inversion of diastereotopic phosphorus atoms with the rate constants for an associated hydride ligand rearrangement in each model also favors Model A over Model B (**Table 1**).

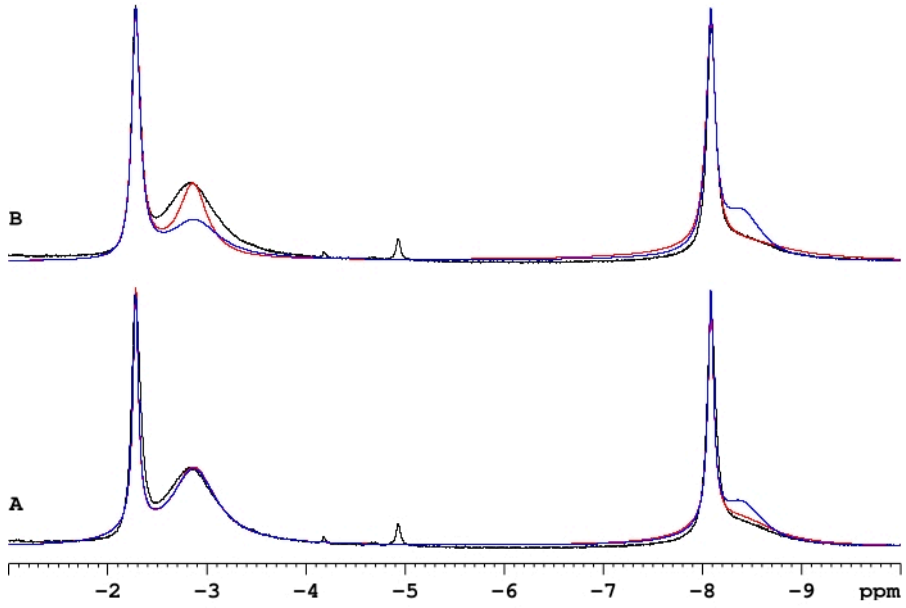

Figure 9. A comparison of two models for the rearrangement of hydride ligands at $ReH_5(PPh_3)_2$(amine) complexes without proton exchange. Both models were tested with the inclusion of an exchange of a specific hydride ligand with a proton from water (red traces) and without such a proton exchange (blue traces). The black traces are the measured ^1H-{^{31}P} NMR spectrum of $ReH_5(PPh_3)_2$(*sec*-butyl amine) at 225 K. The model used to produce the A traces includes a pairwise exchange of A site hydride ligands. The model used to produce the pair of B traces includes a basal turnstile exchange of hydride ligands. Please click here to view a larger version of this figure.

Temperature (K)	k Steric inv. (Hz)	k Pairwise (Hz)	k Basal (Hz)
225	94.5	88.2	6.6
230	131.3	151.3	28.4
235	236	219.3	46.1
240	376.4	324.2	66.4

Table 1. A comparison of rate constants for phosphorus atom steric inversion with pairwise exchange of the A site hydride ligands and with the basal turnstile exchange of hydride ligands. All simulations of hydride resonances included an exchange of protons between adventitious water and the unique B site hydride ligand.

Activation parameters for each modelled dynamic process of Model A can be estimated from Eyring plots (**Figure 10** and **Figure 11**, **Supplementary Figure 6**, and **Supplementary Figure 7**). Eyring plots of dynamic ^{31}P-{^1H} rate constants

have the advantage over Eyring plots of dynamic ^{1}H-{^{31}P} rate constants in that only one model is needed to describe phosphorus atom exchanges. Having a single model for phosphorus atom exchange means that there is no confounding of the phosphorus atom exchange results, unlike hydride ligand exchanges which have multiple exchange models that involve the same atoms. Dynamic ^{31}P-{^{1}H} NMR data is also generally available for a larger range of temperatures than for dynamic ^{1}H-{^{31}P} NMR data which means more data points for the Eyring plot.

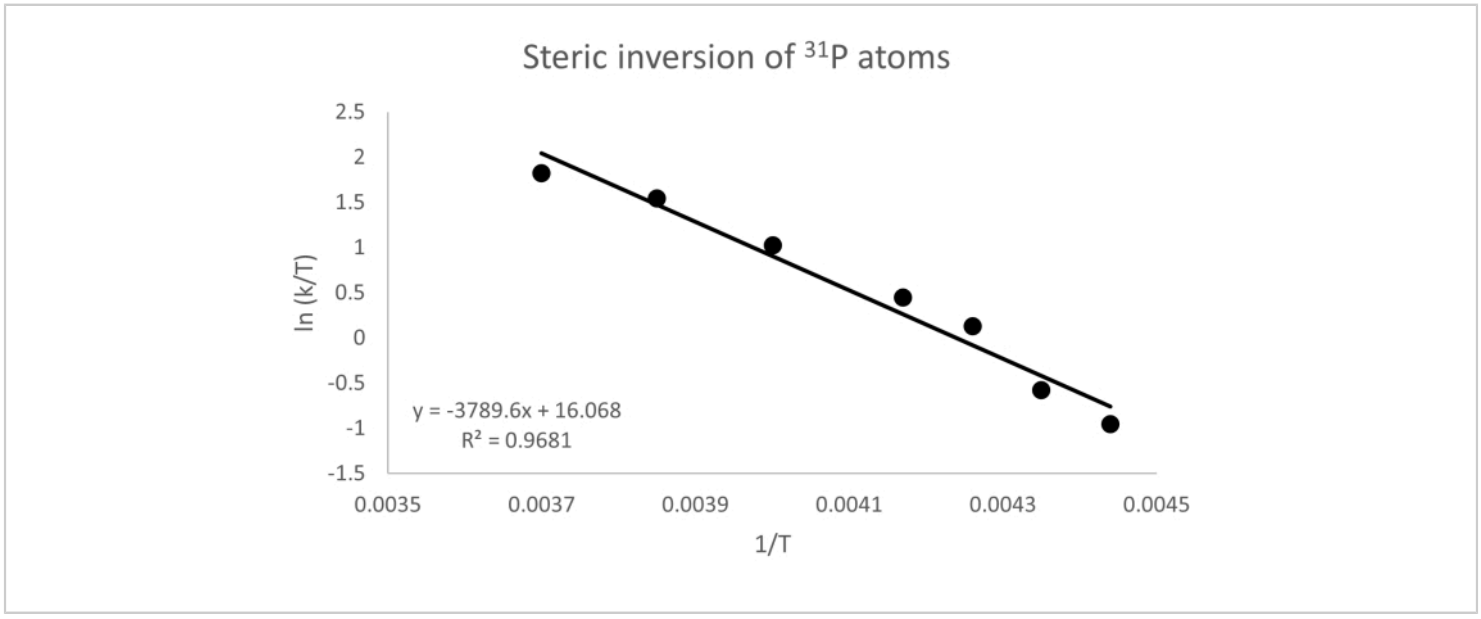

Figure 10. Eyring plot from the line shape fitting of ^{31}P-{^{1}H} NMR spectra for a d$_8$-toluene solution of $ReH_5(PPh_3)_2$(*sec*-butyl amine). The trend line shows that the rate constants that arise from line shape fitting of the ^{31}P-{^{1}H} NMR spectra at several temperatures fit the Eyring equation well. Please click here to view a larger version of this figure.

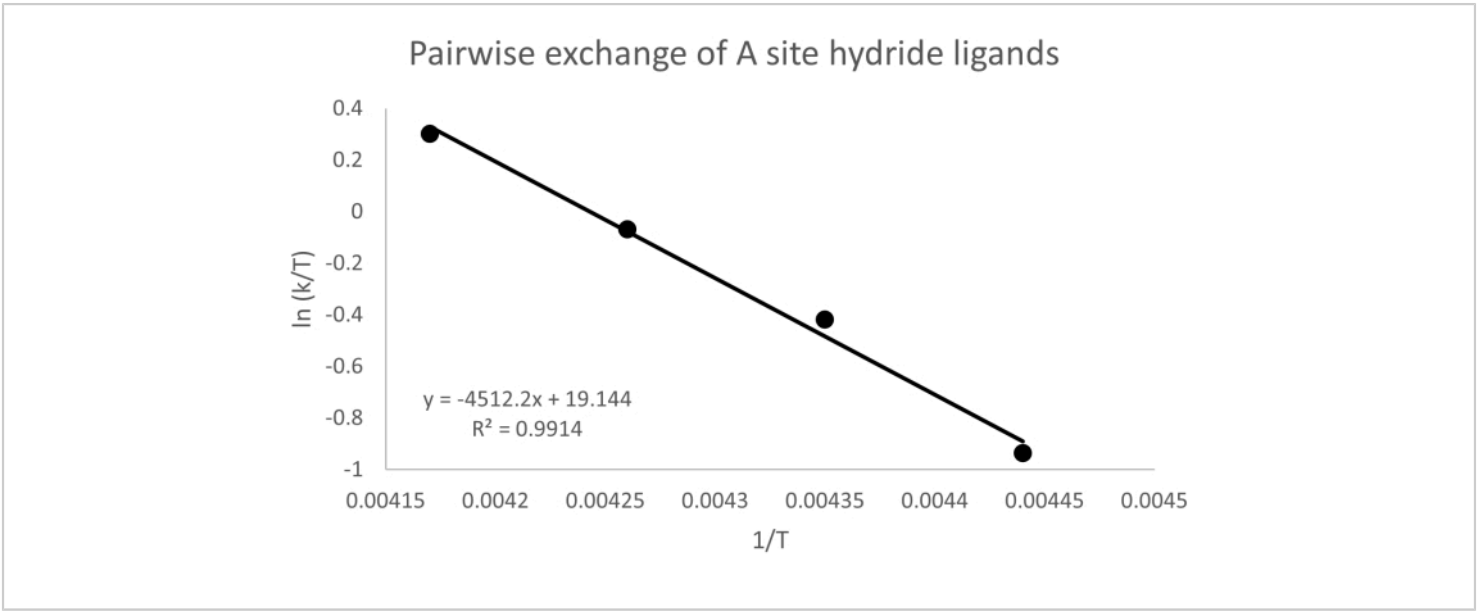

Figure 11. Eyring plot from the pairwise exchange of A site hydride ligands. The data arises from line shape fitting of ^{1}H-{^{31}P} NMR spectra measured on a d_8-toluene solution of $ReH_5(PPh_3)_2$(*sec*-butyl amine). Please click here to view a larger version of this figure.

Supplementary Figure 1: An example of the end point color for the reaction of $ReOCl_3(PPh_3)_2$ with sodium borohydride to form $ReH_7(PPh_3)_2$. The color of the reaction, as shown in the Figure, is the best indication that the reaction between $ReOCl_3(PPh_3)_2$ and sodium borohydride, in tetrahydrofuran and water, has gone to completion. Please click here to download this File.

Supplementary Figure 2. The ^{1}H NMR hydride resonance for a sample of $ReH_7(PPh_3)_2$ dissolved in d_6-benzene. The ^{1}H NMR spectrum of a sample can be used to readily identify the product of a reaction as a genuine sample of $ReH_7(PPh_3)_2$. Please click here to download this File.

Supplementary Figure 3. The ^{31}P-{^{1}H} NMR spectrum of a sample of $ReH_7(PPh_3)_2$ dissolved in d_6-benzene. The ^{31}P-{^{1}H} NMR spectrum can be used to qualitatively characterize a sample of $ReH_7(PPh_3)_2$, and such a spectrum provides a convenient check for impurities in the sample. Please click here to download this File.

Supplementary Figure 4. The room temperature ^{1}H NMR hydride resonance for a sample of $ReH_5(PPh_3)_2$(*sec*-butyl amine) dissolved in d_8-toluene. The small spike on the upfield shoulder of the peak is due to an impurity of $Re_2H_8(PPh_3)_4$. Please click here to download this File.

Supplementary Figure 5. The ^{31}P-{^{1}H} NMR spectrum of a sample of $ReH_5(PPh_3)_2$(*sec*-butyl amine) dissolved in d_8-toluene. The ^{31}P-{^{1}H} NMR spectrum of a sample can be used to qualitatively identify a sample of $ReH_5(PPh_3)_2$(*sec*-

butyl amine) and to check for impurities. Please click here to download this File.

Supplementary Figure 6. Eyring plot from the turnstile exchange of two A site hydride ligands with an adjacent B site hydride ligand. The data arises from line shape fitting of ^{1}H-{^{31}P} NMR spectra measured on a d$_8$-toluene solution of $ReH_5(PPh_3)_2$(*sec*-butyl amine). Please click here to download this File.

Supplementary Figure 7. Eyring plot from the exchange of protons between adventitious water and the unique B site hydride ligand. The data arises from line shape fitting of ^{1}H-{^{31}P} NMR spectra measured on a d$_8$-toluene solution of $ReH_5(PPh_3)_2$(*sec*-butyl amine). Please click here to download this File.

Supplementary Table 1. NMR experiment parameters. Please click here to download this Table.

Discussion

There are four items in the preparation of $ReH_7(PPh_3)_2$ that can impact the quantity and purity of the material that is produced. First, the use of an ice bath during the first 15 min of the reaction is important to remove heat from the reaction that occurs between sodium borohydride and water. Higher initial temperatures lead to a decreased yield of the $ReH_7(PPh_3)_2$ product due to formation of the thermal decomposition product $Re_2H_8(PPh_3)_4$. Second, the color of the reaction mixture is more important than the amount of time for the reaction. When the reaction mixture has gone to completion, the mixture will have a tan to orange color. Any shade of green in the reaction mixture indicates that the reaction must proceed further. If necessary, additional sodium borohydride can be added to the reaction mixture after 1.5 h in case the mixture still has a green color. Third, the washing step is crucial for ensuring a high purity product from the reaction. A thorough water wash ensures that inorganic products such as sodium chloride and sodium borate are washed away from the product. The ethyl ether washes are crucial for removing colored rhenium polyhydride impurities that are always produced in the reaction such as $ReH_5(PPh_3)_3$ and $Re_2H_8(PPh_3)_4$. Finally, the tetrahydrofuran solvent must be peroxide free, which can be accomplished either by using freshly distilled solvent or by storing the solvent under an atmosphere of nitrogen.

For a complex of interest such as $ReH_5(PPh_3)_2$(*sec*-butyl amine), which contains organic-type protons, hydride ligands, and diastereotopic phosphorus atoms, three different variable temperature series of experiments are informative: 1) a series of ^{1}H NMR spectra, 2) a series of ^{1}H-{^{31}P} NMR spectra, and 3) a series of ^{31}P-{^{1}H} NMR spectra. Each of the three different spectra can be acquired sequentially at each temperature of interest. All the dynamic NMR spectra of interest for a complex can be collected on a single NMR sample. The two proton spectra can be measured with 32 K data points for a window of 24 ppm, at 400 MHz, centered at 0 ppm. The phosphorus spectrum can be measured with 32 K data points with a window of 100 ppm, at 162 MHz, centered at 20 ppm. Measuring spectra at temperatures separated by 10 K is usually sufficient for most applications, but increments of 5 K temperature differences obviously produce more data, which can be useful in providing data for an Eyring equation determination of activation parameters. A typical temperature series from room temperature down to 200 K, in increments of 10 K, requires at least consecutive 4 h on the spectrometer. The 4 h include: the time to set up the heat exchanger and bottled nitrogen for the temperature

controller, time for setting up the three experiments that will be measured at each temperature, time to measure room temperature spectra and examine the quality of the sample, time to decrease the temperature in increments of 10 K and stabilize at each temperature, time to shim the sample at each temperature and measure the spectra of interest, and time to warm the sample and spectrometer back to room temperature in increments of 10 K with at least 2 min intervals to stabilize the instrument before again increasing the temperature. Obviously going to lower temperatures or decreasing the temperature increments to 5 K will increase the time required on the spectrometer.

The parameters used for each of the three NMR series in this investigation can be found in the supporting materials. While NMR parameters can be changed during a temperature series, it makes for better comparisons of spectra measured at different temperatures if the spectra are all measured with the same parameters. For $ReH_5(PPh_3)_2$(*sec*-butyl amine) and similar complexes, the temperature series begins in the fast exchange domain. Resonances arising from exchanging nuclei appear as coalesced resonances. Typically, signal-to-noise ratio for the exchanging nuclei will be larger at room temperature and will reach a minimum at a temperature near the coalescence temperature. Due to the changing nature of signal-to-noise, it is best if the signal-to-noise ratio is much better than marginal for the room temperature spectra. Additionally, the acquisition window must be set large enough to include all the resonances that will occur in the slow exchange spectrum.

Complexes of the form $ReH_5(PPh_3)_2$(amine) which include an unsymmetrically substituted aromatic amine such as 3-picoline exhibit *E* and *Z* isomers[9,10]. At lower temperatures where dynamic rearrangements are slowed, phosphorus resonances from both isomers can be observed. Coalescence of these resonances corresponds to observing an average signal from the two interconverting isomers. Since the free energy of the two isomers are not necessarily the same, the phosphorus resonances that arise from these isomers will not necessarily have the same intensities. The line shape fitting software allows for each phosphorus atom in the model to occur in different molecules with different populations. This feature of the line shape fitting software allows for the line shape fitting of $^{31}P\text{-}\{^{1}H\}$ NMR spectra that arise from samples that include *E* and *Z* isomers.

Line shape fitting of the hydride region of the $^{1}H\text{-}\{^{31}P\}$ NMR spectra can be challenging because the individual hydride ligands may participate in multiple dynamic processes. It can be helpful when a chiral center is present, such as occurs with $ReH_5(PPh_3)_2$(*sec*-butyl amine), to compare rate constants for phosphorus atom rearrangement with rate constants for the hydride ligand rearrangements, in order to test whether a hydride ligand rearrangement and a phosphorus atom rearrangement are different manifestations of a single molecular rearrangement. Furthermore, proton exchanges, such as between a hydride ligand and an adventitious water proton (a common occurrence for rhenium polyhydride complexes)[9,13,34] which move a hydride ligand beyond the inner coordination sphere of the metal center, should be readily apparent in line shape fitting as an inability to produce a good fit using models that include only intramolecular hydride ligand exchanges (**Figure 9**)[13].

Rhenium polyhydride complexes serve as pre-catalysts for the transformation of small molecules[23,38,39,40,41,42,43,44,45,46,47,48,49,50,51]. The specific mechanisms for catalytic cycles, though, are generally not well understood. The low activation energy

dynamic processes of such complexes essentially confound all of the atom resonances in room temperature NMR spectra, making the chemical properties of individual atoms in specific locations impossible to follow. Dynamic NMR spectroscopy can allow for the identification of some chemical properties of a specific hydride ligand[9,13]. Catalytic steps with activation energies within the range of 5 to 25 kcal/mol may be apparent with line shape fitting of dynamic NMR spectra of such catalytic systems. Dynamic NMR spectroscopy can also lead to an understanding of dynamic properties, which may lead to rational design of transition metal polyhydride complexes with restricted dynamic properties. Complexes with restricted dynamic properties should allow for room temperature NMR investigations of chemical properties of specific atoms in specific coordination sites and lead to insight into catalytic cycles that start with transition metal polyhydride complexes.

Disclosures

The authors have no conflicts of interest to disclose.

Acknowledgments

The authors thank the Department of Chemistry and Physics and the Creativity and Research Grant Program (Naik, Moehring) at Monmouth University for financial support of this work.

References

1. Zimmer, K. D., Shoemaker, R., Ruminski, R. R. Synthesis and characterization of a fluxional Re(I) carbonyl complex *fac*-[Re(CO)$_3$(dpop')Cl] with the nominally tri-dentate ligand dipyrido(2,3-α:3',2'-j)phenazine (dpop'). *Inorganica Chimica Acta.* **359** (5), 1478-1484 (2006).
2. McGlinchey, M. J. Symmetry breaking in NMR spectroscopy: the elucidation of hidden molecular rearrangement processes. *Symmetry.* **6** (3), 622-654 (2014).
3. Casarini, D., Luazzi, L., Mazzanti, A. Recent advances in stereodynamics and conformational analysis by dynamic NMR and theoretical calculations. *European Journal of Organic Chemistry.* **2010** (11), 2035-3056 (2010).
4. Palmer, A. G., Williams, J., McDermott, A. Nuclear magnetic resonance studies of biopolymer dynamics. *Journal of Physical Chemistry.* **100** (31), 13293-13310 (1996).
5. Kern, D., Kern, G., Scherer, G., Fischer, G., Drakenberg, T. Kinetic analysis of cyclophilin-catalyzed prolyl cis/trans isomerization by dynamic NMR spectroscopy. *Biochemistry.* **34** (41), 13594-13602 (1995).
6. Menger, F. M., Lynn, J. L. Fast proton transfer at a micelle surface. *Journal of the American Chemical Society.* **97** (4), 948-949 (1975).
7. Pines, A., Rabinovitz, M. A nuclear magnetic resonance total line-shape treatment of internal rotation in dimethylformamide. *Tetrahedron Letters.* **9** (31), 3529-3532 (1968).
8. Mancinelli, M., Bencivenni, G., Pecorari, D., Mazzanti, A. Stereochemistry and recent applications of axially chiral organic molecules. *European Journal of Organic Chemistry.* **2020** (27), 4070-4086 (2020).
9. Streisel, D. J. et al. Fluxionality, substitution, and hydrogen exchange at eight-coordinate rhenium(V) polyhydride centers. *Inorganica Chimica Acta.* **496** (1), 119028 (2019).
10. Jimenez, Y., Strepka, A. M., Borgohain, M. D., Hinojosa, P. A., Moehring, G. A. *Ortho*-metalation, rotational isomerization, and hydride-hydride coupling

at rhenium(V) polyhydride complexes stabilized by aromatic amine ligands. *Inorganica Chimica Acta.* **362** (9), 3259-3266 (2009).

11. Lee Jr., J. C., Yao, W., Crabtree, R. H., Ruegger, H. Fluxionality in [$ReH_5(PPh_3)_2$(pyridine)]. *Inorganic Chemistry.* **35** (3), 695-699 (1996).
12. Patel, B. P., Kavallieratos, K., Crabtree, R. H. Effects of dihydrogen bonding on fluxionality in $ReH_5(PPh_3)_2L$. *Journal of Organometallic Chemistry.* **528** (1), 205-207 (1997).
13. Geetha, B. et al. Chiral amine ligands at rhenium(V) pentahydride complexes allow for characterization of an energetically accessible and reversible steric inversion of diastereotopic phosphorus atoms. *Inorganica Chimica Acta.* ***531*** (1), .120741 (2022).
14. Paulo, A., Ascenso, J., Domingos, A., Galvao, A., Santos, I. Rhenium-(III) and -(V) hydride complexes with modified poly(pyrazolyl)borates. *Journal of the Chemical Society, Dalton Transactions.* **1999** (8), 1293-1300 (1999).
15. Bianchini, C. et al. Synthesis and characterization of rhenium polyhydrides stabilized by the tripodal ligand $MeC(CH_2PPh_2)_3$. *Journal of Organometallic Chemistry.* **451** (1), 97-106 (1993).
16. Scorzelli, A. G., Macalush, B. E., Naik, D. V., Moehring, G. A. Comparative study of fluxional processes at two different classes of eight-coordinate rhenium(V) polyhydride complexes. *Inorganica Chimica Acta.* **516** (1), 120120 (2021).
17. Luo, X.-L., Crabtree, R. H. Synthesis and spectroscopic characterization of rhenium complexes [ReH_5(triphos)] and [ReH_6(triphos)]$^+$ [triphos = $PPh(CH_2CH_2PPh_2)_2$]. *Journal of the Chemical Society, Dalton Transactions.* **1991** (5), 587-590 (1991).
18. Kim, Y., Deng, H., Gallucci, J. C., Wojcicki, A. Rhenium polyhydride complexes containing $PhP(CH_2CH_2CH_2PCy_2)_2$ (Cyttp): protonation, insertion, and ligand substitution reactions of ReH_5(Cyttp) and structural characterization of ReH_5(Cyttp) and [$ReH_4(\eta^2\text{-}H_2)$(Cyttp)]SbF_6. *Inorganic Chemistry.* **35** (24), 7166-7173 (1996).
19. Bolano, S. et al. Synthesis, characterization, protonation studies and X-ray crystal structure of $ReH_5(PPh_3)_2$(PTA) (PTA = 1,3,5-triaza-7-phosphaadamantane). *Journal of Organometallic Chemistry.* **691** (4), 629-637 (2006).
20. Ginsberg, A. P., Abrahams, S. C., Jamieson, P. B. Nonrigid stereochemistry in eight-coordinate pentahydridorhenium complexes. *Journal of the American Chemical Society.* **95***(14), 4751.*-4752 (1973).
21. Bolano, S., Bravo, J., Garcia-Fontan, S. Mono- and dinuclear rhenium polyhydride complexes bearing the chelating ligand 1,2-bis(dicyclohexylphosphinanyloxy)ethane. *European Journal of Inorganic Chemistry.* **2004** (24), 4812-4819 (2004).
22. Leeaphon, M., Rohl, K., Thomas, R. J., Fanwick, P. E., Walton, R. A. Reactions of the polyhydride complex $ReH_7(PPh_3)_2$ with quinoline, 2-hydroxyquinoline, and 2-mercaptoquinoline. The preparation and characterization of hydrido complexes of rhenium(V) and chloro complexes of rhenium(III). *Inorganic Chemistry.* **32** (24), 5562-5568 (1993).

23. Mejia, E., Togni, A. Rhenium complexes containing the chiral tridentate ferrocenyl ligand pigiphos. *Organometallics.* ***30***. (17), 4765-4770 (2011).

24. Moehring G. A., Walton, R. A. Reactions of heptahydrobis(triphenylphosphine)rhenium with bidentate aromatic heterocycles. *Inorganic Chemistry.* **26** (17), 2910-2912 (1987).

25. Kosanovich, A. J., Reibenspies, J. H., Ozerov, A. V., Complexes of high-valent rhenium supported by the PCP pincer. *Organometallics.* **35** (4), 513-519 (2016).

26. Emge, T. J., Koetzle, T. F., Bruno, J. W., Caulton, K. G. Pentahydridorhenium: crystal and molecular structure of $ReH_5(PMePh_2)_3$. *Inorganic Chemistry.* **23** (24), 4012-4017 (1984).

27. Costello, M. T., Fanwick, P. E., Green, M. A., Walton, R. A. Reactions of Heptahydridobis(triphenylphosphine)rhenium with 1-(diphenylphosphino)-2-(diphenylarsino)ethane (arphos) and 1,2-bis(diphenylarsino)ethane (dpae). Structural characterization of $ReH_5(PPh_3)_2$(arphos-As) and $ReH_5(PPh_3)_2$(dpae-As). *Inorganic Chemistry.* **30** (4), 861-864 (1991).

28. Alvarez Jr., D., Lundquist, E. G., Ziller, J. W., Evans, W. J., Caulton, K. G. Synthesis, structure and applications of transition-metal polyhydride anions. *Journal of the American Chemical Society.* **111** (22), 8392-8398 (1989).

29. Albinati, A. et al. Synthesis, characterization, and interconversion of the rhenium polyhydrides $[ReH_3(\eta^4\text{-}NP_3)]$ and $[ReH_4(\eta^4\text{-}NP_3)]^+$ {NP_3 = tris[2-(diphenylphosphanyl)ethyl]amine}. *European Journal of Inorganic Chemistry.* **2002** (6), 1530-1539 (2002).

30. Bosque, R. et al. Site preference energetics, fluxionality, and intramolecular M−H···H−N hydrogen bonding in a dodecahedral transition metal polyhydride. *Inorganic Chemistry.* **36** (24), 5505-5511 (1997).

31. Tao, Y., Sou, W., Luo, G.-G., Kraka, E. Describing polytopal rearrangement processes of octacoordinate structures. I. renewed insights into fluxionality of the rhenium polyhydride complex $ReH_5(PPh_3)_2$(Pyridine). *Inorganic Chemistry.* **60** (4), 2492-2502 (2021).

32. Beringhelli, T., D'Alfonso, G., Minoja, A. P. Rhenium-platinum mixed metal clusters. Characterization in solution and dynamic behavior of the isomers of $[Re_3Pt(\mu\text{-}H_3)(CO)_{14}]$. An example of a labile metal fragment that undergoes intermolecular exchange. *Organometallics.* **13** (2), 663-668 (1994).

33. Grieco, G. Blacque, O. Solution and solid-state structure of the first NHC-substituted rhenium heptahydrides. *European Journal of Inorganic Chemistry.* **2019** (34), 3810-3819 (2019).

34. Wazio, J. A., Jimenez, V., Soparawalla, S., John, S., Moehring, G. A. Hydrogen exchange of rhenium(VII) heptahydridobis(triphenylphosphine) with water, aniline, methanol, and itself. *Inorganica Chimica Acta.* **362** (1), 159-165 (2009).

35. Chatt, J., Coffey, R. S. Hydrido-complexes of rhenium-containing tertiary phosphines *Journal of the Chemical Society, A.* **1969** (0), 1963-1972 (1969).

36. Tao, Y., Wang, X., Zou, W., Luo, G.-G., Kraka, E. Unusual intramolecular motion of ReH_9^{2-} in K_2ReH_9 crystal: circle dance and three-arm turnstile mechanisms revealed by computational study. *Inorganic Chemistry.* **61** (2), 1041-1050 (2022).

37. Berger, X., Braun, S. *200 and More NMR Experiments a Practical Course.* Wiley-VCH, Weinheim, Federal Republic of Germany (2004).

38. He, G., Chen, J., Sung, H. H.-Y., Williams, I. D., Jia, G. Substituent effect on reactions of $ReH_5(PMe_2Ph)_3$ with propargyl alcohols. *Inorganica Chimica Acta.* **518** (1), 120239 (2021).

39. Donnelly, L. J., Parsons, S., Morrison, C. A., Thomas, S. P., Love, J. B. Synthesis and structures of anionic rhenium polyhydride complexes of boron-hydride ligands and their application in catalysis. *Chemical Science.* **11** (9), 9994-9999 (2020).

40. Donnelly, L. J. et al. C-H borylation catalysis of heteroaromatics by a rhenium boryl polyhydride. *ACS Catalysis.* **11** (12), 7394-7400 (2021).

41. Jin, H. et al. CO-enabled rhenium hydride catalyst for directed C(sp^2)-H bond alkylation with olefins. *Organic Chemistry Frontiers.* **2** (4), 378-382 (2015).

42. Takaya, H., Ito, M., Murahashi, S.-I. Rhenium-catalyzed addition of carbonyl compounds to the carbon−nitrogen triple bonds of nitriles: α-C−H activation of carbonyl compounds. *Journal of the American Chemical Society.* **131** (31), 10824-10825 (2009).

43. Carr, S. W., Fowles, E. H., Fontaine, X. L. R., Shaw, B. L. Multihydride complexes of rhenium, osmium or iridium containing monodentate ditertiary phosphine ligands: selective hydrogen-deuterium exchanges of the rhenium multihydrides. *Journal of the Chemical Society, Dalton Transactions.* **1990** (2), 573-579 (1990).

44. Jin, H. et al. Rhenium-catalyzed acceptorless dehydrogenative coupling via dual activation of alcohols and carbonyl compounds. *ACS Catalysis.* **3** (10), 2195-2198 (2013).

45. Loza, M. L., de Gala, S., Crabtree, R. H. Steric crowding in a rhenium polyhydride induced by a chelating disilyl ligand: synthesis, characterization, and reactivity of $ReH_5(disil)(PPh_3)_2$ (disil = 1,2-Bis(dimethylsilyl)benzene and 1,2-Bis(dimethylsilyl)ethane). *Inorganic Chemistry.* **33** (22), 5073-5078 (1994).

46. Lin, Y., Zhu, X., Xiang, M. Transition metal polyhydrides-catalyzed addition of activated nitriles to aldehydes and ketones via Knoevenagel condensation. *Journal of Organometallic Chemistry.* **448** (1-2), 215-218 (1993).

47. Abdukader, A., Jin, H., Cheng, Y., Zhu, C. Rhenium-catalyzed amination of alcohols by hydrogen transfer process. *Tetrahedron Letters.* **55** (30), 4172-4174 (2014).

48. Lin, Y., Zhou, Y. Selective transfer hydrogenation catalyzed by transition metal polyhydrides. *Fenzi Cuihua.* **5** (2) 119-124 (1991).

49. Green, M. A., Huffman, J. C., Caulton, K. G., Rybak, W. K., Ziolkowski, J. J. Ligand scavenging and catalytic utilization of the phototransient $ReH_5(PMe_2Ph)_2$. *Journal of Organometallic Chemistry.* **218** (2), C39-C43 (1981).

50. Komiya, S., Chigira, T., Suzuki, T., Hirano, M. Polymerization of alkyl methacrylate catalyzed by hydridorhenium complexes. *Chemistry Letters.* **1999** (4) 347-348 (1999).

51. Michos, D., Luo, X. L., Faller, J. W., Crabtree, R. H. Tungsten(VI) hexahydride complexes supported by chelating triphosphine ligands: protonation to give η^2-

dihydrogen complexes and catalytic dehydrogenation of cyclooctane to cyclooctene. *Inorganic Chemistry*. **32** (8), 1370-1375 (1993).